ACS OMEGA

http://pubs.acs.org/journal/acsodf

Article

A Novel Tin-Doped Titanium Oxide Nanocomposite for Efficient Photo-Anodic Water Splitting

Manzar Sohail,* Nadeem Baig, Muhammad Sher, Rabia Jamil, Muhammad Altaf, Sultan Akhtar, and Muhammad Sharif*

Cite This: *ACS Omega* 2020, 5, 6405−6413

Read Online

ACCESS | Metrics & More | Article Recommendations | Supporting Information

ABSTRACT: Herein, we report the expedient synthesis of new nanocomposite $Sn_{0.39}Ti_{0.61}O_2{\cdot}TiO_2$ flakes using simple sol−gel and calcination methods. In order to prepare this material, first, we generated a polymeric gel using cost-effective and easily accessible precursors such as $SnCl_4$, titanium isopropoxide, and tetrahydrofuran (THF). A small amount of triflic acid was used to initiate THF polymerization. The calcination of the resulting gel at 500 °C produced a Sn−Ti bimetallic nanocomposite. This newly synthesized $Sn_{0.39}Ti_{0.61}O_2{\cdot}TiO_2$ was characterized by X-ray diffraction (XRD), energy-dispersive X-ray spectroscopy (EDX), scanning electron microscopy (SEM), transmission electron microscopy (TEM), and UV−visible spectroscopy. The photoelectrochemical (PEC) studies were performed for the first time using $Sn_{0.39}Ti_{0.61}O_2{\cdot}TiO_2$ coated over fluorine-doped tin oxide (FTO) under simulated 1 sun solar radiation. The chronoamperometric study of the $Sn_{0.39}Ti_{0.61}O_2{\cdot}TiO_2$/FTO revealed the repeatable and substantially higher photocurrent for the oxygen evolution reaction (OER) when compared to only TiO_2. Moreover, the synthesized material exhibited high stability both in the presence and absence of light. The photocatalytic studies suggested that the sol−gel-synthesized $Sn_{0.39}Ti_{0.61}O_2{\cdot}TiO_2$ can be efficiently used as a photoanode in the water-splitting reaction.

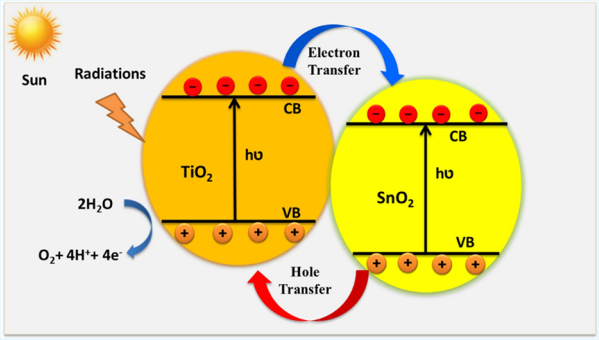

1. INTRODUCTION

Nanomaterials represent highly privileged class of advanced materials, which become increasingly important[1,2] in a diverse range of fields such as energy, catalysis, sensing, drug delivery, and painting technology.[3] Although the number of such materials is literarily unknown, still the development of novel and cost-effective new materials for valued application is highly desired. In particular, the preparation of low-cost nanocomposite materials continues to be a major challenge and is crucial for the advancement of chemical processes related to academic research and industrial production.[4−6] Photoelectrochemical (PEC) water splitting is among the most promising approaches in artificial photosynthesis and a potential alternative of fossil fuels. PEC splitting of water was first reported by Fujishima and Honda in 1972 using TiO_2 as a catalyst.[7−9] Since then, a tremendous amount of work has been reported on PEC water splitting with several nanocomposite catalysts. PEC water splitting utilizes a semiconducting photocathode for H_2 evolution (HER) and/or a photoanode for O_2 evolution (OER) reactions, making it a convenient way to convert solar energy into renewable fuels that can be easily transferred and transported.[10] Among these two reactions, OER is more challenging as it requires 4 moles of electrons per one mole of oxygen produced. For the development of commercially viable devices, one of the crucial challenges is the design of a photoanode with higher efficiency and stability. For water-splitting photocatalysts, one of the major challenges is photocorrosion of the electrodes. Some of the photogenerated holes and electrons do not participate in the oxidation/reduction of water and instead initiate the decomposition of the electrode itself.[11]

One of the most commonly applied photoactive materials is titanium dioxide; it got attention due to its chemical inertness, photostability, nontoxicity, and cost-effectiveness. However, the higher band gap of TiO_2 puts a limitation on its PEC application. Due to its high band gap, it absorbs sunlight only in the ultraviolet (UV) region. Natural light consists of just a small portion of UV light (4−5%), while the visible region ranging from 400 to 800 nm is the major part of sunlight.[12,13] The photocatalytic effect generated by absorption of the photon results in the creation of the hole−electron (h^+/e^-)

Received: November 13, 2019
Accepted: January 30, 2020
Published: March 18, 2020

pairs.[14] The anatase TiO_2 upon exposure to the UV light produces a good photoresponse.[15] However, nonmodified anatase TiO_2 absorbs only a small fraction of light for the h^+/e^- pair generation, and also, recombination of h^+/e^- pairs is fast. Overall, the TiO_2 thin-film photoelectrode's low photocurrent might be due to the lethargic electrons' movement to the rear of the electrodes, recombination of electron and hole pairs, and poor electrical conductivity.[16]

More recently, a number of other materials including WO_3, Fe_2O_3, $CuWO_4$, $BiVO_4$, and SnO_2 have been used as photoanodes.[17−25] However, the photochemical efficiency of the individual aforementioned semiconductors is low because of fast charge recombination occurring at the interface and surface, leading to low charge transfer and thus lowering the energy conversion.

Among various metallic oxides, the SnO_2 can be proven as an excellent photoanode material due to its promising features of low cost, intrinsic stability, excellent charge mobility (100−200 $cm^2\ V^{-1}\ s^{-1}$), and high electron transfer efficiency.[26] However, pure SnO_2-based photoanodes exhibit low photocatalytic activity even under UV light because of the small surface to volume ratio, low light capture efficiency, and a large band gap. To address these issues, different semiconducting materials with large surface areas such as nanosheets, nanowires, and nanotubes have been used as a photoanode to improve the light-harvesting ability and active surface area for the electrochemical reaction. The porous anodic tin oxide films fabricated by the Sn anodization and annealing have displayed better PEC performance in the visible region.[27] As discussed, the SnO_2 possessed better conductivity, nearly two orders of magnitude compared to pure TiO_2.[27] The combination of SnO_2 with other nanomaterials displays different band gaps or Fermi levels, which can improve the PEC performance of the composite material. The SnO_2 and TiO_2 bilayer structures were used to develop effective heterojunction photoelectrodes.[17] Similarly, a lot of efforts have been made on the modification of semiconductors such as TiO_2 to improve their PEC behavior either by impurity doping or semiconductor coupling.[28,29]

Recently, numerous heterostructured semiconductor−TiO_2 thin films including $CdS{\cdot}TiO_2$,[30−32] $ZnO{\cdot}TiO_2$,[33,34] $FeS_2{\cdot}TiO_2$,[35] and $SnO_2{\cdot}TiO_2$[36] have been developed as photoelectrodes. Among these doped nanocomposites, the Sn- or SnO_2-doped TiO_2 is getting great attention in photocatalysis.[37,38] This system is widely being explored to improve the PEC behavior of hybrid materials for enhanced water splitting. The doping of Sn^{2+} or Sn^{+4} is receiving consideration especially for TiO_2 as a small mismatch in the lattice of the TiO_2 and SnO_2 provides good structural stability and compatibility. Sn doping in TiO_2 is considered more effective compared to the other dopings due to the rough similarities of the Sn^{+4} (0.690 Å) and Ti^{+4} (0.605 Å).[39,40] At the interface, the mixed cation nanocomposite $Sn_xTi_{1-X}O_2$ can facilitate the excitation by modulating the electronic properties and thus provide a better charge separation.[41] SnO_2 and TiO_2 features are different as SnO_2 has greater electron mobility and its conduction band is lower than TiO_2.[42] A combination of SnO_2 and TiO_2 imparts unique characteristics to the hybrid material. These electronic properties of $SnO_2{\cdot}TiO_2$ hybrid heterojunction can allow the photogenerated electrons in the TiO_2 conduction band migrate to SnO_2, while photogenerated holes in the SnO_2 valence band migrate to the TiO_2.[43] Various chemical routes are being adopted for tin doping into TiO_2 to enhance the photoactivity of the composite.[36,44] $Ti_{1-x}Sn_xO_2$ nanocrystalline materials were synthesized by Fresno et al. in which Sn^{4+} doping was reported with both anatase and rutile phases of TiO_2. It was observed that the presence of Sn^{4+} changes the structural and electronic properties. $Ti_{1-x}Sn_xO_2$ nanocrystals showed better photocatalytic activity for oxidative decomposition of oxidation of methylcyclohexane dye.[45] Chua et al. reported the synthesis of thin films of anatase TiO_2 with 3.4% Sn^{4+} doping through aerosol-assisted chemical vapor deposition. Sn^{4+}-doped anatase displayed 10% enhanced photocatalytic efficiency for stearic acid degradation owing to the decreased rate of electron−hole recombination.[46] Arunachalam et al. synthesized Sn^{4+}-doped TiO_2 porous indium tin oxide electrodes by spray pyrolysis and showed that Sn^{4+}-doped TiO_2 electrodes showed better photocatalytic activities with a decreased band gap.[47] Chandra et al. synthesized polythiophene over Sn^{4+}-doped TiO_2 and studied that polythiophene performed better for LPG sensitivity due to better photocatalytic activity of Sn^{4+}-doped TiO_2.[48] In this work, we report on the synthesis of a bimetallic $Sn_{0.39}Ti_{0.61}O_2{\cdot}TiO_2$ nanocomposite using a facile and more convenient sol−gel method and for the first time reported its PEC activity for the OER reaction.

2. RESULTS AND DISCUSSION

2.1. Structural Characterization and Morphological Studies of the Sn−Ti Nanocomposite. Figure 1 presents

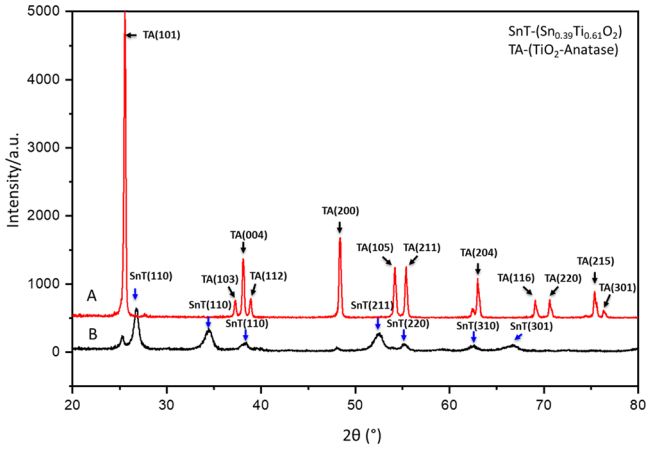

Figure 1. XRD patterns of (A) TiO_2 anatase and (B) $Sn_{0.39}Ti_{0.61}O_2{\cdot}TiO_2$ nanocomposites

the pXRD diffraction pattern of $Sn_{0.39}Ti_{0.61}O_2{\cdot}TiO_2$, which was characterized by ICDD-BD card no. 01-076-8392 for tin−titanium ($Sn_{0.39}Ti_{0.61}O_2$) and ICDD-BD card no. 01-075-2544 for titania (TiO_2) in anatase form. The ratio between $Sn_{0.39}Ti_{0.61}O_2$ and TiO_2 was found to be 82.5 and 17.5% by a relative intensity ratio (RIR) analysis method (Figure S1). The TiO_2 anatase displayed its characteristics XRD peaks (Figure 1A) at 25.5° (101), 38.3° (004), 48.3° (200), 54.1° (105), 55.4° (211), 63.1° (204), 69.1° (116), 70.6° (220), and 74.5° (215).[49] $Sn_{0.39}Ti_{0.61}O_2$ was characterized by major peaks present at 26.8° (110), 34.5° (101), and 52.8° (211), while $Sn_{0.39}Ti_{0.61}O_2{\cdot}TiO_2$ was characterized by peaks at 25.3°, 38.3°, and 47.9° (Figure 1B). All other small peaks also belonged to either $Sn_{0.39}Ti_{0.61}O_2$ or anatase TiO_2. The crystallite size calculated by the Debye−Scherer method for $Sn_{0.39}Ti_{0.61}O_2$ ranged from 8−11 nm, while for anatase TiO_2, it was found in

https://dx.doi.org/10.1021/acsomega.9b03876
ACS Omega 2020, 5, 6405−6413

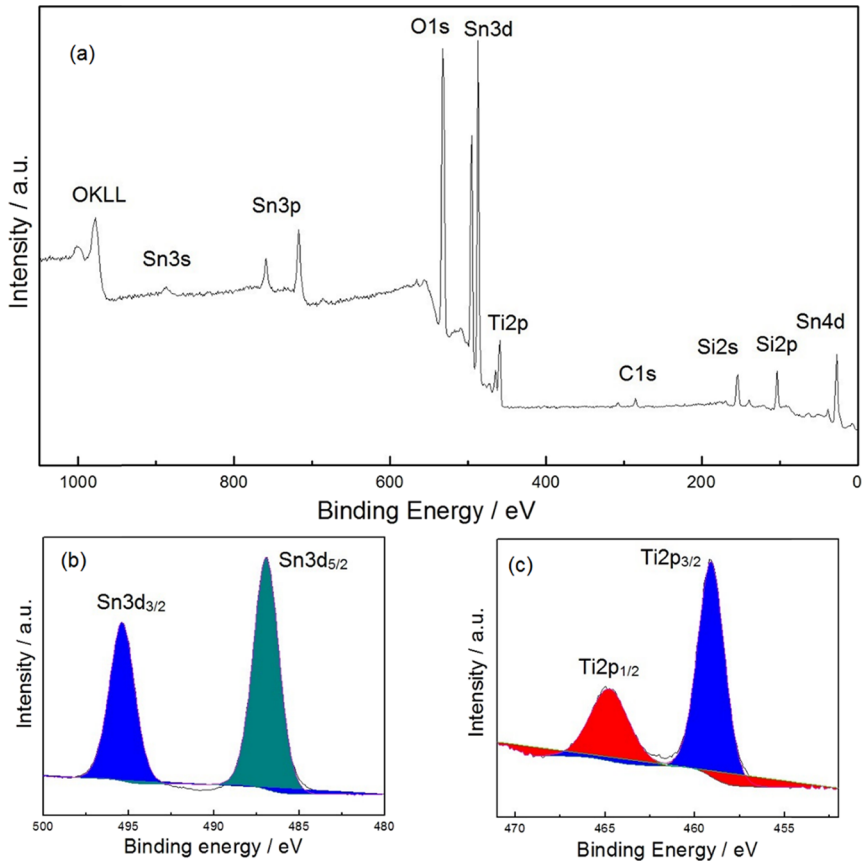

Figure 2. XPS spectra of the $Sn_{0.39}Ti_{0.61}O_2.TiO_2$: (a) Survey scan and high resolution (b) Sn $3d_{5/2}$ and Sn $3d_{3/2}$, (c) Ti $2p_{3/2}$ and Ti $2p_{1/2}$ states.

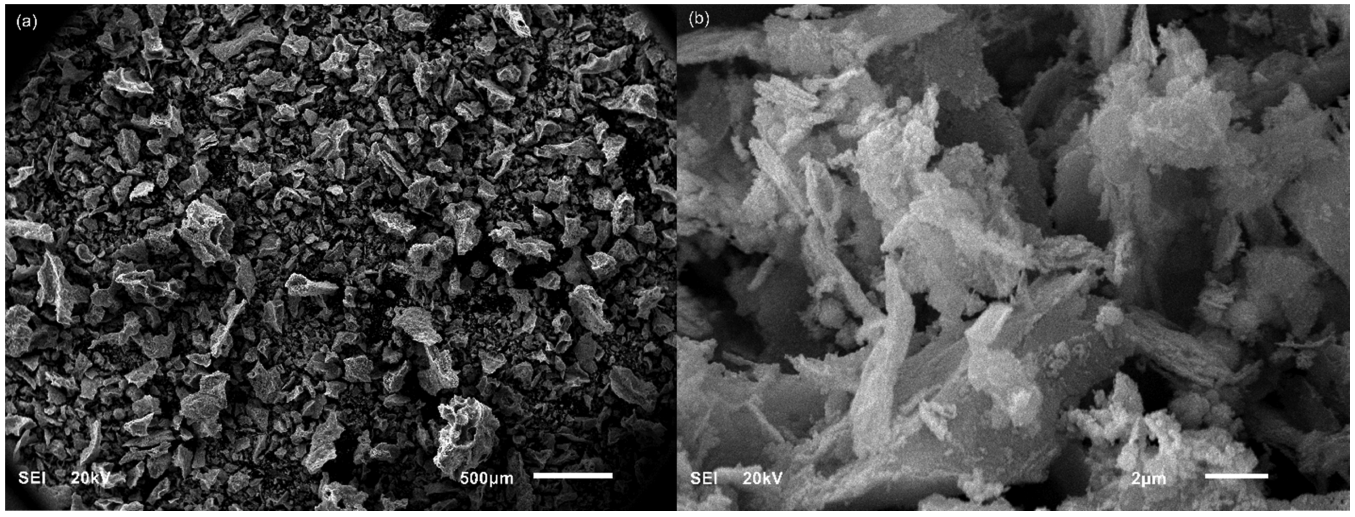

Figure 3. FESEM images of the synthesized $Sn_{0.39}Ti_{0.61}O_2.TiO_2$ composite at different magnifications: (a) 500 μm and (b) 2 μm. The composite $Sn_{0.39}Ti_{0.61}O_2{\cdot}TiO_2$ emerged as flakes of varying thicknesses.

between 9−14 nm. The synthesized photoactive composite $Sn_{0.39}Ti_{0.61}O_2$ has displayed small-sized nanoparticles compared to the anatase TiO_2 nanoparticles. Furthermore, it is evident from the substantial reduction of the XRD peak intensity of the photoactive composite $Sn_{0.39}Ti_{0.61}O_2$ compared to the XRD spectrum of the anatase TiO_2.

Sn-doped titanium oxide was further investigated by XPS spectroscopy to get the information of bonding composition. The survey scan XPS spectra of the synthesized material revealed the various electronic orbital signatures of Ti $2p_{3/2,\ 1/2}$, Sn $3d_{5/2,\ 3/2}$ O 1s, and C 1s (Figure 2). The carbon signal might be due to residual C produced during calcination. The binding energy of the C 1s main peak was adjusted to 284.8 eV for compensating sample charging, and all other peaks were corrected accordingly (Figure S2). The well resolved two characteristics peaks $Ti2p_{3/2}$ and $Ti2p_{1/2}$ and $Sn3d_{5/2}$ and $Sn3d_{3/2}$ were observed in the XPS spectra. XPS spectra (Figure 2b) demonstrate two distinguish peaks of the Sn $3d_{5/2}$ and $3d_{3/2}$ at 486.668 and 495.190 eV, respectively. The binding energy difference between two peaks of Sn was 8.522 eV.

https://dx.doi.org/10.1021/acsomega.9b03876
ACS Omega 2020, 5, 6405−6413

Typically, in the XPS spectra of Ti 2p, peaks appear at 458.6 eV ($2p_{3/2}$)and 464.4 eV ($2p_{1/2}$). As presented in Figure 2c, the doping of Sn into TiO_2 imparted a blueshift at 464.686 eV. The blueshift in the binding energy was 0.404 eV and 0.286 eV, respectively. This change in binding energy was an indication of successful doping of Sn atoms into the TiO_2 instead of just being present at the surface. In Sn-doped TiO_2, the O 1s spectra's prominent peak appeared at 532.274 eV. However, O 1s spectra also revealed another peak at 530.624 eV, which indicated the presence of two types of O present in the nanocomposite (Figure S3).

The surface morphology of the synthesized tin-doped titanium oxide composite was revealed by field-emission scanning electron microscopy (FESEM). SEM images were evaluated at different magnifications as shown by Figure 3a,b. It was clearly observed that the tin-doped titanium oxide composite demonstrated the flake-like morphology with varying sizes and thicknesses.

Energy-dispersive X-ray spectroscopy (EDX) study was performed to confirm the elemental existence of the synthesized tin-doped titanium oxide nanocomposite as shown in Figure S4. EDX mapping study of the synthesized composite demonstrates the uniform distribution of the Sn in the TiO_2 (Figure S4a). The uniform distribution of the Sn, Ti, and O can be seen in Figure S4b−d, indicating the equal ratio of elements in the composite lattice. The mapping of the $Sn_{0.39}Ti_{0.61}O_2{\cdot}TiO_2$ also revealed that the Sn is successfully incorporated into the TiO_2. No data was found for the impurity elements, which proved the pure preparation of the tin-doped titanium oxide nanocomposite. The EDX spectrum (Figure S4e) revealed the presence of Sn, Ti, and O in the synthesized $Sn_{0.39}Ti_{0.61}O_2{\cdot}TiO_2$ flakes. Elemental analysis and EDX elemental mapping images show comparable results. ICP elemental mapping analysis shows 40.8% Sn and 16.9% Ti, while EDX shows 39.6% Sn and 16.8% Ti. FESEM examination, EDX mapping, and EDS elemental results altogether confirmed the successful preparation of the $Sn_{0.39}Ti_{0.61}O_2{\cdot}TiO_2$ composite via a sol−gel route.

Transmission electron microscopy (TEM) was carried out to evaluate the surface morphology and structure of synthesized $Sn_{0.39}Ti_{0.61}O_2{\cdot}TiO_2$ flakes at high resolution. Figure 4 shows the TEM image of one of the tin-based titanium oxide flakes along with the electron diffraction pattern. It was clear that the composite was showing flake-like morphology with almost a uniform thickness as judged by the same contrast. The TEM image further revealed that the flake consisted of smaller particles in the range of 10−20 nm. The particle size of 10−20 nm and crystallite size calculated from pXRD demonstrated that particles consisted of 1−2 crystallites. These nanoparticles collected together and consequently shaped the flake-like morphology. These nanoflakes displayed the crystalline nature when selected-area electron diffraction pattern (SAED) was recorded from the flake region (Figure 4b). The SAED pattern showed the ring patterns where each ring was indexed as (started from the inner ring) 110, 101, 211, 022, etc. in agreement with XRD data.

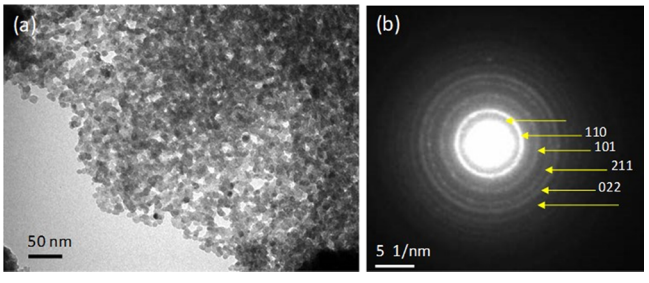

Figure 4. (a)TEM image of the $Sn_{0.39}Ti_{0.61}O_2{\cdot}TiO_2$ composite along with the SAED pattern. The nanocomposite composed of individual particles in the range of 10−20 nm. (b) SAED pattern displaying the crystalline structure of the composite. The major reflections are indexed as 110, 101, 211, and 022.

The Brunaur−Emmet−Teller (BET) method was used to determine the surface area, size of pores, and their distribution. The BET surface area found was 120 m^2/g with an average pore diameter of 8.28 nm, and a pore volume of 0.000915 cm^3/g was obtained. These results are comparable to the high-surface-area anatase reported in the literature.[50,51] See Figure S6.

2.2. UV−Visible Study of the $Sn_{0.39}Ti_{0.61}O_2{\cdot}TiO_2$ Composite. The synthesized photoactive material was further investigated by UV−visible spectroscopy. The analysis of UV−visible spectroscopy facilitates the band gap energy estimation of Sn-doped TiO_2. For UV−visible analysis, the material was scanned from 200 to 800 nm. The synthesized material demonstrated an absorbance from 550 to 200 nm. The absorbance capability was enhanced as λ was moving from 550 to 200 nm (Figure 5a). From the absorbance curve, the cut off wavelength was found at 395 nm. The band gap energy calculated using eq 1 was 3.14 eV. Furthermore, the band gap energy calculation was done using diffused reflectance spectroscopy (Figure 5b). The band gap energy was further verified by using the Tauc equation and Kubelka−Munk equation.[52] The band gap value was calculated at about 3.11 eV. This value is very close to the UV−visible calculated value of 3.14 eV. This band gap was slightly lower than the band gap of pure TiO_2 (~3.2 eV).

2.3. PEC Investigation of the $Sn_{0.39}Ti_{0.61}O_2{\cdot}TiO_2$ Composite. For PEC investigation of the synthesized material, the FTO electrode was drop-casted with the $Sn_{0.39}Ti_{0.61}O_2{\cdot}TiO_2$ as a thin film at the surface of the electrode. The PEC behavior of the $Sn_{0.39}Ti_{0.61}O_2{\cdot}TiO_2$/FTO electrode was explored under 1 sun solar simulator light presence and absence by dipping in a 0.5 M Na_2SO_4 electrolyte. First of all, the LSV was scanned by switching on and off the light simulator, and it was found that the current was enhanced significantly under light and returned back to the background value as the light was turned off. This behavior of the material revealed that $Sn_{0.39}Ti_{0.61}O_2{\cdot}TiO_2$ was photosensitive (Figure 6).

The background current was also enhanced as the potential was increased beyond 0.5 V. Chronoamperometry was applied to observe the reproducibility and stability of the $Sn_{0.39}Ti_{0.61}O_2{\cdot}TiO_2$/FTO electrode for OER. In chronoamperometry, the current density (J) was recorded at a specific time interval by controlling the on/off mode of the light simulator. The sharp spike of the current was observed as the light was switched on, and after a certain time, the current was leveled off. The photocurrent was increased to 210 μA from about 0 μA when the light was turned on, indicating that the OER started when the light struck the $Sn_{0.39}Ti_{0.61}O_2{\cdot}TiO_2$ surface. The photoanodic current density was sharply decreased, close to the background current, when the light was turned off (Figure 7a). However, under the same set of conditions, TiO_2

https://dx.doi.org/10.1021/acsomega.9b03876
ACS Omega 2020, 5, 6405−6413

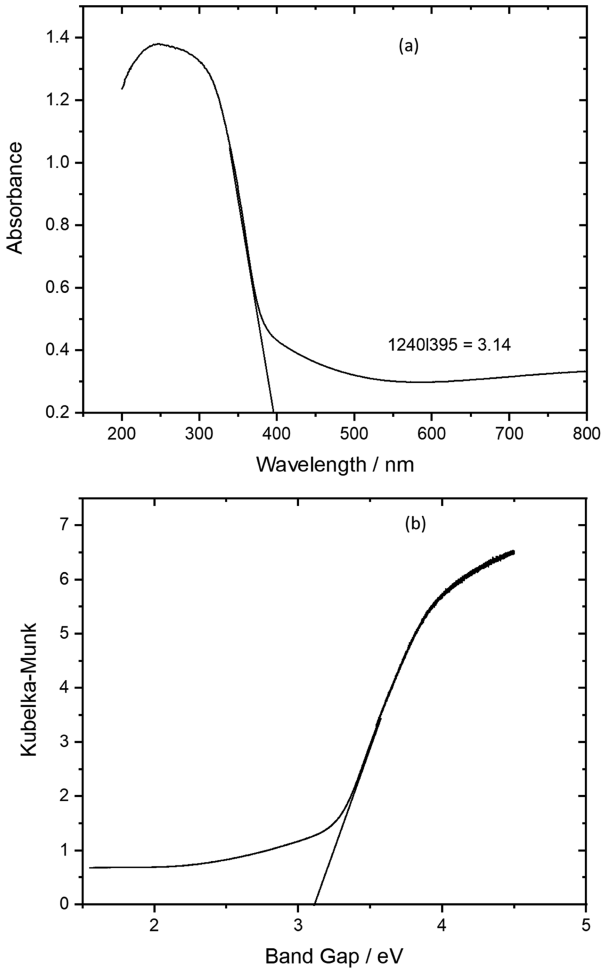

Figure 5. (a) UV−visible spectra of $Sn_{0.39}Ti_{0.61}O_2{\cdot}TiO_2$ from 200 to 900 nm and (b) Kubelka−Munk plot from diffused spectra of $Sn_{0.39}Ti_{0.61}O_2{\cdot}TiO_2$ for calculation of the band gap.

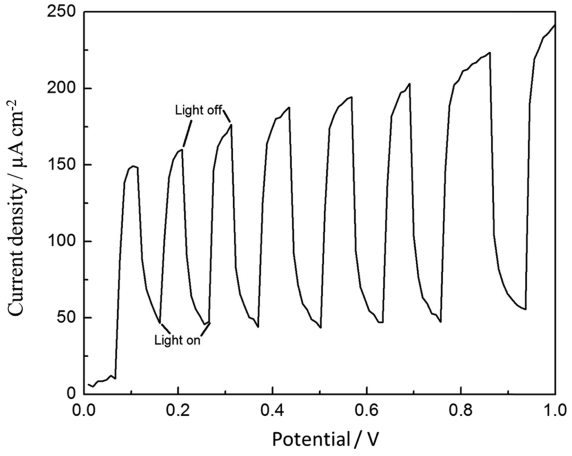

Figure 6. LSV curve recorded with the $Sn_{0.39}Ti_{0.61}O_2{\cdot}TiO_2$/FTO electrode for the OER reaction under chopping light mode.

anatase/FTO has displayed a poor photoelectrochemical response. The maximum current displayed by the TiO_2 anatase/FTO photoelectrode under light was 0.05 μA (Figure S5), which was extremely lower compared to the $Sn_{0.39}Ti_{0.61}O_2.TiO_2$/FTO electrode photocurrent (210 μA) for OER. The photoelectrochemical analysis of the TiO_2

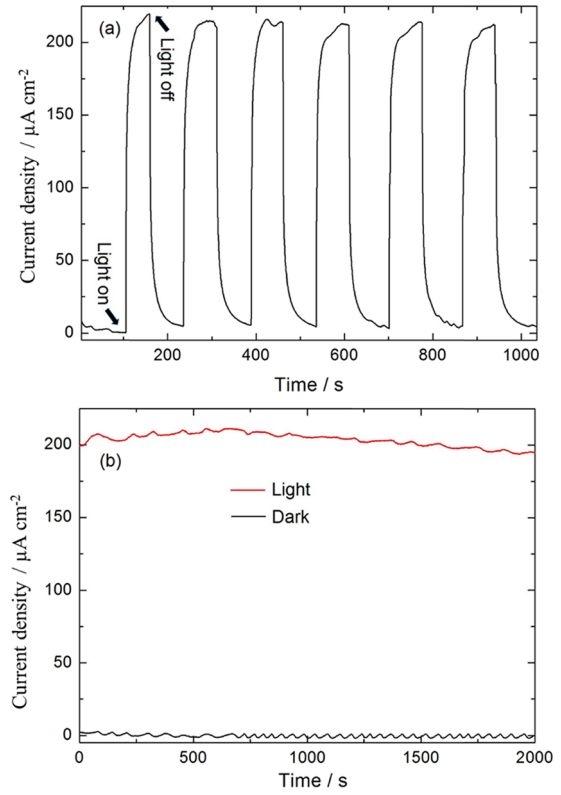

Figure 7. . (a) Chronoamperometery in light chopping mode and (b) stability of the $Sn_{0.39}Ti_{0.61}O_2{\cdot}TiO_2$/FTO response for the OER reaction under dark and light.

anatase/FTO and $Sn_{0.39}Ti_{0.61}O_2{\cdot}TiO_2$/FTO electrodes have revealed that the resultant composite ($Sn_{0.39}Ti_{0.61}O_2{\cdot}TiO_2$), by doping of the Sn into TiO_2, has substantially improved the photoelectrochemical performance of the photoelectrode. This behavior of the Sn-doped TiO_2 demonstrated that this nanocomposite is highly sensitive toward light.

The stability of the $Sn_{0.39}Ti_{0.61}O_2{\cdot}TiO_2$/FTO photoanode was also tested under dark and under 1 sunlight illumination as displayed in Figure 7b. The dark current was very stable, while only a slight reduction in photocurrent was observed over more than 30 min of testing time due to O_2 evolution and accumulation of O_2 bubbles at the $Sn_{0.39}Ti_{0.61}O_2{\cdot}TiO_2$/FTO surface.

2.4. Possible Mechanism of OER on the $Sn_{0.39}Ti_{0.61}O_2{\cdot}TiO_2$ Photoanode. The doping of Sn into TiO_2 has provided a better charge separation in the photoactive material. The interface of the TiO_2 and SnO_2 facilitates the separation of the hole and electrons by providing the alternate positions for them. The mechanism of the charge separation at the interface of TiO_2/SnO_2 was proposed in Figure 8. The band gap of SnO_2 is wider than TiO_2. However, it is interesting that the conduction band (CB) of the SnO_2 appeared lower than the conduction band of TiO_2. Similarly, the valence band (VB) of the TiO_2 appeared above the VB of the SnO_2. As the light radiations strike on the interface of the TiO_2/SnO_2, the holes generated during the active state started to migrate from the VB of SnO_2 to TiO_2. Similarly, the electrons moved from the CB of TiO_2 to SnO_2 during the excitation state. This phenomenon has provided the effective separation of the electron−hole pair and increased the lifetime by suppressing their recombination (Figure 8). This is according to the

https://dx.doi.org/10.1021/acsomega.9b03876
ACS Omega 2020, 5, 6405−6413

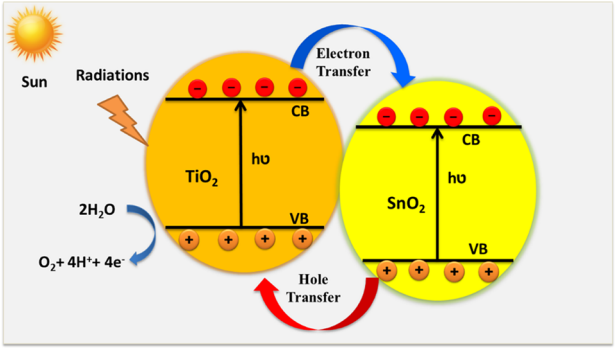

Figure 8. . Schematic illustration of the photoelectrochemical reaction on the photoanode $Sn_{0.39}Ti_{0.61}O_2{\cdot}TiO_2$-coated FTO.

literature that the potential difference among SnO_2 and TiO_2 permitted the facile migration of photoelectrons from the TiO_2 to SnO_2 CB.[53] Moreover, the mixed cation composition $Sn_{0.39}Ti_{0.61}O_2{\cdot}TiO_2$ accelerates the exciton generation and separation, which enhanced the photocurrent.

3. MATERIALS AND METHODS

3.1. Characterization of the Nanocomposite. The XRD patterns were recorded using a Smart Lab X-ray diffractometer (Rigaku, Japan) with Cu-Kα X-ray radiations (λ = 0.15406 nm). X-ray photoelectron spectroscopy (XPS) was carried out with an ESCALAB 250Xi, Thermo Scientific, UK instrument. The adventitious carbon peak that appeared at a binding energy of 284.8 eV was used as a reference. A UV/vis−NIR spectrometer by "Agilent Cary series" was used for determination of optical properties. Scanning electron microscopy (SEM) and energy-dispersive X-ray (EDS) analysis were carried out by a field-emission scanning electron microscope (FESEM; Tescan Lyra-3) equipped with a focused ion beam (FIB) and energy-dispersive spectroscopic (EDS) detector. The TEM analysis of the synthesized composite was performed using a transmission electron microscope (TEM; FEI, Morgagni 268, Czech Republic). Selected-area electron diffraction (SAED) patterns in TEM were recorded to evaluate the structure of the nanocomposite and confirm the XRD data. A TEM sample was dispersed in ethanol and deposited onto a Cu grid holding a holey carbon film. SEM and TEM instruments were operated at working potentials of 20 and 80 kV, respectively. For surface area determination, a Micromeritics (ASAP model) BET analyzer (Micromeritics Headquarters, 4356 Communications Drive, Norcross, GA 30093-2901, U.S.) was used. Before the measurement of surface area, the sample was kept under N_2 flow at 250 °C for 5 h to remove moisture and other adsorbed gases. Then N_2 adsorption/desorption was performed at 77 K using a liquid nitrogen bath.

3.2. Optical Band Gap Determination. The band gap energy was calculated using the following equation

$$E = h \times C/\lambda \quad (1)$$

where E is the band gap energy (eV), h is Planck's constant (6.626×10^{-34} J/s), C is the light speed (3.0×10^8 m/s), and λ is the cut off wavelength (nm). Furthermore, the band energy calculation was done using diffused reflectance spectroscopy (Figure 5b). The band gap energy was further verified by using the Tauc equation and Kubelka−Munk equation.[52] The following Tauc equation (eq 2) was used for the calculation of the band gap energy

$$(\alpha h\nu)^n = A(h\nu - E_g) \quad (2)$$

where α is the absorption coefficient, h represents Planck's constant, A is a constant, ν represents the frequency, E_g represents the band gap, and the n value is $^1/_2$ for the direct allowed transition.

The Kubelka−Munk equation (eq 3) was used for the calculation of the absorption coefficient (α) by using the diffuse reflectance.

$$F(R) = (1 - R)^2/2R = k/s \quad (3)$$

In eq 3, R represents the absolute reflectance, s represents the scattering coefficient, and k represents the molar absorption coefficient. The Kubelka−Munk function $F(R)$ was calculated by using the assimilated diffuse reflectance spectrum that was equivalent to the absorption coefficient (α). The obtained quantity $[F(R)h\nu]$ 0.5 was plotted against the photon energy ($h\nu$) to obtain the band gap energy. The linear part of the curve was extended to obtain the band gap value.

3.3. Synthesis of $Sn_{0.39}Ti_{0.61}O_2{\cdot}TiO_2$. Tin chloride, titanium isopropoxide, triflic acid (TFC), and tetrahydrofuran (THF) were obtained from Sigma-Aldrich and used without any purification. The detailed synthesis procedure of $Sn_{0.39}Ti_{0.61}O_2{\cdot}TiO_2$ along several other new nanocomposites has been reported recently.[54] Briefly, tin(IV) chloride and titanium isopropoxide as precursors for the $Sn_{0.39}Ti_{0.61}O_2{\cdot}TiO_2$ composite were added to 25 mL of tetrahydrofuran (THF), and polymerization of THF was initiated by adding 0.5 mL of triflic acid (TFC) as shown in the equation. In a 50 mL round-bottom flask, tin(IV) chloride pentahydrate (0.01 M, 0.043 mL) and titanium isopropoxide (0.01 M, 3.03 mL) were mixed in 25 mL of THF at 25 °C. Then, 0.5 mL of TFC was added to initiate the polymerization of THF. Slow polymerization of THF was allowed to occur with constant stirring at 25 °C for 4 h. After the formation of polymeric gel, whole reaction products were transferred to a crucible and placed in a furnace. The calcination was performed by raising the temperature to 500 °C at a rate of 4 °C per min and held there for 2 h. After pyrolysis, the catalytic material was cooled to room temperature and stored in glass vials.

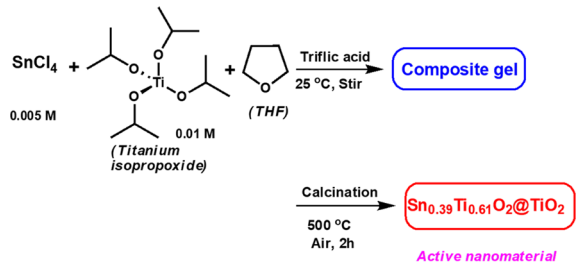

3.4. PEC Studies of the Nanocomposite. The PEC measurements were carried out by a conventional three-electrode system in 1 M Na_2SO_4 (pH = 7) as a supporting electrolyte. The working electrode was an FTO glass coated with 200 μL of 2% nafion suspension of the composite $Sn_{0.39}Ti_{0.61}O_2{\cdot}TiO_2$; Pt gauze served as an auxiliary electrode and the standard Ag/AgCl/3 M KCl as a reference electrode (SCE). All the PEC experiments were performed using a Metrohm Autolab potentiostat (PGSTAT302N) instrument. For solar light in the laboratory, an Oriel Sol3A class AAA solar simulator (Newport) with the following specifications were

https://dx.doi.org/10.1021/acsomega.9b03876
ACS Omega 2020, 5, 6405−6413

used: power of 100 mW cm^{-2} (1 sun), IEC/JIS/ASTM-certified, containing a 450 W xenon lamp, Air Mass 1.5G Filter, UV cut off the filter and 2 × 2 in aperture for output beam.

4. CONCLUSIONS

A new sol−gel method is introduced for the synthesis of the photoactive catalyst for PEC splitting of water. The $Sn_{0.39}Ti_{0.61}O_2{\cdot}TiO_2$ catalyst was synthesized by utilizing the acid-catalyzed ring-opening polymerization of THF. The attractive features of the synthetic route of the catalyst are its simple methodology and a potential to synthesize several other nanocomposite materials. The $Sn_{0.39}Ti_{0.61}O_2{\cdot}TiO_2$ was characterized using SEM, TEM, EDX, XRD, UV−visible spectroscopy, voltammetry, and chronoamperometry. The structure characterization confirmed the formation of $Sn_{0.39}Ti_{0.61}O_2{\cdot}TiO_2$ with successful doping of Sn^{+4} into TiO_2. The combination of the VB and CB of the SnO_2 and the TiO_2 in the nanocomposite provided a heterojunction displaying a great capability to harvest natural light for efficient splitting of water. The $Sn_{0.39}Ti_{0.61}O_2{\cdot}TiO_2$ demonstrated good stability under both light and dark conditions. This material may prove to be a good addition as a photoanode for PEC water splitting.

ASSOCIATED CONTENT

Supporting Information

The Supporting Information is available free of charge at https://pubs.acs.org/doi/10.1021/acsomega.9b03876.

Relative intensity ratio analysis from pXRD, C 1s high-resolution XPS spectrum, O 1s high-resolution XPS spectrum, EDX mapping images and spectrum, chronoamperometery in light chopping mode of TiO_2, and BET adsorption−desorption isotherm graph for $Sn_{0.39}Ti_{0.61}O_2{\cdot}TiO_2$ (PDF)

AUTHOR INFORMATION

Corresponding Authors

Manzar Sohail − *Department of Chemistry, School of Natural Sciences, National University of Sciences and Technology, Islamabad 45320, Pakistan*; orcid.org/0000-0003-1457-2491; Phone: +92-51-9058-5596; Email: Manzar.sohail@sns.nust.edu.pk

Muhammad Sharif − *Chemistry Department, King Fahd University of Petroleum and Minerals, Dhahran 31261, Saudi Arabia*; Email: msharif@kfupm.edu.sa

Authors

Nadeem Baig − *Chemistry Department and Center for Research Excellence in Desalination and Water Treatment, King Fahd University of Petroleum and Minerals, Dhahran 31261, Saudi Arabia*

Muhammad Sher − *Department of Chemistry, Allama Iqbal Open University, Islamabad 44000, Pakistan*

Rabia Jamil − *Department of Chemistry, School of Natural Sciences, National University of Sciences and Technology, Islamabad 45320, Pakistan*

Muhammad Altaf − *Department of Chemistry, Government College University, Lahore 54000, Pakistan*

Sultan Akhtar − *Electron Microscopy Unit, Institute for Research and Medical Consultations, Imam Abdulrahman Bin Faisal University, Dammam 31441, Saudi Arabia*

Complete contact information is available at: https://pubs.acs.org/10.1021/acsomega.9b03876

Notes

The authors declare no competing financial interest.

REFERENCES

(1) Corma, A.; Garcia, H. Supported gold nanoparticles as catalysts for organic reactions. *Chem. Soc. Rev.* **2008**, *37*, 2096−2126.

(2) Sharma, N.; Ojha, H.; Bharadwaj, A.; Pathak, D. P.; Sharma, R. K. Preparation and catalytic applications of nanomaterials: a review. *RSC Adv.* **2015**, *5*, 53381−53403.

(3) Wegener, S. L.; Marks, T. J.; Stair, P. C. Design Strategies for the Molecular Level Synthesis of Supported Catalysts. *Acc. Chem. Res.* **2012**, *45*, 206−214.

(4) Gawande, M. B.; Branco, P. S.; Varma, R. S. Nano-magnetite (Fe_3O_4) as a support for recyclable catalysts in the development of sustainable methodologies. *Chem. Soc. Rev.* **2013**, *42*, 3371−3393.

(5) Huber, D. L. Synthesis, Properties, and Applications of Iron Nanoparticles. *Small* **2005**, *1*, 482−501.

(6) Gomes Silva, C.; Juárez, R.; Marino, T.; Molinari, R.; García, H. Influence of Excitation Wavelength (UV or Visible Light) on the Photocatalytic Activity of Titania Containing Gold Nanoparticles for the Generation of Hydrogen or Oxygen from Water. *J. Am. Chem. Soc.* **2011**, *133*, 595−602.

(7) Fujishima, A.; Honda, K. Electrochemical Photolysis of Water at a Semiconductor Electrode. *Nature* **1972**, *238*, 37.

(8) Gholamrezaei, S.; Ghanbari, M.; Amiri, O.; Salavati-Niasari, M.; Foong, L. K. $BaMnO_3$ nanostructures: Simple ultrasonic fabrication and novel catalytic agent toward oxygen evolution of water splitting reaction. *Ultrason. Sonochem.* **2020**, *61*, 104829.

(9) Gholamrezaei, S.; Salavati-Niasari, M. Sonochemical synthesis of $SrMnO_3$ nanoparticles as an efficient and new catalyst for O_2 evolution from water splitting reaction. *Ultrason. Sonochem.* **2018**, *40*, 651−663.

(10) Hisatomi, T.; Kubota, J.; Domen, K. Recent advances in semiconductors for photocatalytic and photoelectrochemical water splitting. *Chem. Soc. Rev.* **2014**, *43*, 7520−7535.

(11) Jiang, C.; Moniz, S. J. A.; Wang, A.; Zhang, T.; Tang, J. Photoelectrochemical devices for solar water splitting − materials and challenges. *Chem. Soc. Rev.* **2017**, *46*, 4645−4660.

(12) Shaban, Y. A.; Khan, S. U. M. Visible light active carbon modified n-TiO_2 for efficient hydrogen production by photoelectrochemical splitting of water. *Int. J. Hydrogen Energy* **2008**, *33*, 1118−1126.

(13) Zhang, Z.; Zhang, L.; Hedhili, M. N.; Zhang, H.; Wang, P. Plasmonic Gold Nanocrystals Coupled with Photonic Crystal Seamlessly on TiO_2 Nanotube Photoelectrodes for Efficient Visible Light Photoelectrochemical Water Splitting. *Nano Lett.* **2013**, *13*, 14−20.

(14) Park, J. H.; Kim, S.; Bard, A. J. Novel carbon-doped TiO_2 nanotube arrays with high aspect ratios for efficient solar water splitting. *Nano Lett.* **2006**, *6*, 24−28.

(15) Sopha, H.; Krbal, M.; Ng, S.; Prikryl, J.; Zazpe, R.; Yam, F. K.; Macak, J. M. Highly efficient photoelectrochemical and photocatalytic anodic TiO_2 nanotube layers with additional TiO_2 coating. *Appl. Mater. Today* **2017**, *9*, 104−110.

(16) Kim, J. S.; Kim, Y. B.; Baek, S. K.; Yun, Y. D.; Jung, S. H.; Cho, S. W.; Ahn, C. H.; Cho, H. K. Compositionally graded SnO_2/TiO_2 bilayered compounds with dramatically enhanced charge transport efficiency for self-driven water purification applications. *J. Alloys Compd.* **2019**, *776*, 839−849.

(17) Khan, M. D.; Aamir, M.; Sohail, M.; Sher, M.; Baig, N.; Akhtar, J.; Malik, M. A.; Revaprasadu, N. Bis(selenobenzoato)dibutyltin(iv) as a single source precursor for the synthesis of SnSe nanosheets and their photo-electrochemical study for water splitting. *Dalton Trans.* **2018**, *47*, 5465−5473.

(18) Han, H. S.; Shin, S.; Noh, J. H.; Cho, I. S.; Hong, K. S. Heterojunction Fe_2O_3-SnO_2 Nanostructured Photoanode for Efficient Photoelectrochemical Water Splitting. *JOM* **2014**, *66*, 664−669.

https://dx.doi.org/10.1021/acsomega.9b03876
ACS Omega 2020, 5, 6405−6413

(19) Lee, Y.-L.; Chi, C.-F.; Liau, S.-Y. CdS/CdSe Co-Sensitized TiO_2 Photoelectrode for Efficient Hydrogen Generation in a Photoelectrochemical Cell. *Chem. Mater.* **2010**, *22*, 922−927.
(20) Su, J.; Feng, X.; Sloppy, J. D.; Guo, L.; Grimes, C. A. Vertically Aligned WO3 Nanowire Arrays Grown Directly on Transparent Conducting Oxide Coated Glass: Synthesis and Photoelectrochemical Properties. *Nano Lett.* **2011**, *11*, 203−208.
(21) Sivula, K.; le Formal, F.; Grätzel, M. Solar Water Splitting: Progress Using Hematite (α-Fe_2O_3) Photoelectrodes. *ChemSusChem* **2011**, *4*, 432−449.
(22) Yourey, J. E.; Pyper, K. J.; Kurtz, J. B.; Bartlett, B. M. Chemical Stability of $CuWO_4$ for Photoelectrochemical Water Oxidation. *J. Phys. Chem. C* **2013**, *117*, 8708−8718.
(23) Su, J.; Guo, L.; Yoriya, S.; Grimes, C. A. Aqueous Growth of Pyramidal-Shaped $BiVO_4$ Nanowire Arrays and Structural Characterization: Application to Photoelectrochemical Water Splitting. *Cryst. Growth Des.* **2010**, *10*, 856−861.
(24) He, H.; Berglund, S. P.; Rettie, A. J. E.; Chemelewski, W. D.; Xiao, P.; Zhang, Y.; Mullins, C. B. Synthesis of $BiVO_4$ nanoflake array films for photoelectrochemical water oxidation. *J. Mater. Chem. A* **2014**, *2*, 9371−9379.
(25) Ghanbari, M.; Salavati-Niasari, M. Tl_4CdI_6 Nanostructures: Facile Sonochemical Synthesis and Photocatalytic Activity for Removal of Organic Dyes. *Inorg. Chem.* **2018**, *57*, 11443−11455.
(26) Zhang, Z.; Gao, C.; Wu, Z.; Han, W.; Wang, Y.; Fu, W.; Li, X.; Xie, E. Toward efficient photoelectrochemical water-splitting by using screw-like SnO_2 nanostructures as photoanode after being decorated with CdS quantum dots. *Nano Energy* **2016**, *19*, 318−327.
(27) Zaraska, L.; Gawlak, K.; Gurgul, M.; Chlebda, D. K.; Socha, R. P.; Sulka, G. D. Controlled synthesis of nanoporous tin oxide layers with various pore diameters and their photoelectrochemical properties. *Electrochim. Acta* **2017**, *254*, 238−245.
(28) Ansari, S. A.; Cho, M. H. Highly Visible Light Responsive, Narrow Band gap TiO_2 Nanoparticles Modified by Elemental Red Phosphorus for Photocatalysis and Photoelectrochemical Applications. *Sci. Rep.* **2016**, *6*, 25405.
(29) Jang, J. S.; Ahn, C. W.; Won, S. S.; Kim, J. H.; Choi, W.; Lee, B.-S.; Yoon, J.-H.; Kim, H. G.; Lee, J. S. Vertically Aligned Core−Shell $PbTiO_3$@TiO_2 Heterojunction Nanotube Array for Photoelectrochemical and Photocatalytic Applications. *J. Phys. Chem. C* **2017**, *121*, 15063−15070.
(30) Zhao, D.; Yang, C.-F. Recent advances in the TiO_2/CdS nanocomposite used for photocatalytic hydrogen production and quantum-dot-sensitized solar cells. *Renewable Sustainable Energy Rev.* **2016**, *54*, 1048−1059.
(31) Liu, Y.; Zhou, H.; Zhou, B.; Li, J.; Chen, H.; Wang, J.; Bai, J.; Shangguan, W.; Cai, W. Highly stable CdS-modified short TiO_2 nanotube array electrode for efficient visible-light hydrogen generation. *Int. J. Hydrogen Energy* **2011**, *36*, 167−174.
(32) Daskalaki, V. M.; Antoniadou, M.; Li Puma, G.; Kondarides, D. I.; Lianos, P. Solar Light-Responsive Pt/CdS/TiO_2 Photocatalysts for Hydrogen Production and Simultaneous Degradation of Inorganic or Organic Sacrificial Agents in Wastewater. *Environ. Sci. Technol.* **2010**, *44*, 7200−7205.
(33) Momeni, M. M.; Ghayeb, Y. Visible light-driven photoelectrochemical water splitting on ZnO−TiO_2 heterogeneous nanotube photoanodes. *J. Appl. Electrochem.* **2015**, *45*, 557−566.
(34) Pan, K.; Dong, Y.; Zhou, W.; Pan, Q.; Xie, Y.; Xie, T.; Tian, G.; Wang, G. Facile Fabrication of Hierarchical TiO_2 Nanobelt/ZnO Nanorod Heterogeneous Nanostructure: An Efficient Photoanode for Water Splitting. *ACS Appl. Mater. Interfaces* **2013**, *5*, 8314−8320.
(35) Xin, Y.; Li, Z.; Wu, W.; Fu, B.; Zhang, Z. Pyrite FeS_2 Sensitized TiO_2 Nanotube Photoanode for Boosting Near-Infrared Light Photoelectrochemical Water Splitting. *ACS Sustainable Chem. Eng.* **2016**, *4*, 6659−6667.
(36) Radecka, M.; Wnuk, A.; Trenczek-Zajac, A.; Schneider, K.; Zakrzewska, K. TiO_2/SnO_2 nanotubes for hydrogen generation by photoelectrochemical water splitting. *Int. J. Hydrogen Energy* **2015**, *40*, 841−851.
(37) Sayılkan, F.; Asiltürk, M.; Tatar, P.; Kiraz, N.; Şener, Ş.; Arpaç, E.; Sayılkan, H. Photocatalytic performance of Sn-doped TiO_2 nanostructured thin films for photocatalytic degradation of malachite green dye under UV and VIS-lights. *Mater. Res. Bull.* **2008**, *43*, 127−134.
(38) Vinodgopal, K.; Bedja, I.; Kamat, P. V. Nanostructured Semiconductor Films for Photocatalysis. Photoelectrochemical Behavior of SnO_2/TiO_2 Composite Systems and Its Role in Photocatalytic Degradation of a Textile Azo Dye. *Chem. Mater.* **1996**, *8*, 2180−2187.
(39) Mehraz, S.; Kongsong, P.; Taleb, A.; Dokhane, N.; Sikong, L. Large scale and facile synthesis of Sn doped TiO_2 aggregates using hydrothermal synthesis. *Sol. Energy Mater. Sol. Cells* **2019**, *189*, 254−262.
(40) Mahanty, S.; Roy, S.; Sen, S. Effect of Sn doping on the structural and optical properties of sol−gel TiO_2 thin films. *J. Cryst. Growth* **2004**, *261*, 77−81.
(41) Pan, J.; Hühne, S.-M.; Shen, H.; Xiao, L.; Born, P.; Mader, W.; Mathur, S. SnO_2−TiO_2 Core−Shell Nanowire Structures: Investigations on Solid State Reactivity and Photocatalytic Behavior. *J. Phys. Chem. C* **2011**, *115*, 17265−17269.
(42) McCool, N. S.; Swierk, J. R.; Nemes, C. T.; Schmuttenmaer, C. A.; Mallouk, T. E. Dynamics of Electron Injection in SnO_2/TiO_2 Core/Shell Electrodes for Water-Splitting Dye-Sensitized Photoelectrochemical Cells. *J. Phys. Chem. Lett.* **2016**, *7*, 2930−2934.
(43) Shi, H.; Zhou, M.; Song, D.; Pan, X.; Fu, J.; Zhou, J.; Ma, S.; Wang, T. Highly porous SnO_2/TiO_2 electrospun nanofibers with high photocatalytic activities. *Ceram. Int.* **2014**, *40*, 10383−10393.
(44) Yusoff, M. M.; Mamat, M. H.; Malek, M. F.; Abdullah, M. A. R.; Ismail, A. S.; Saidi, S. A.; Mohamed, R.; Suriani, A. B.; Khusaimi, Z.; Rusop, M. Sn-doped TiO_2 nanorod arrays produced by facile one step aqueous chemical route: Structural characterization. *AIP Conf. Proc.* **2018**, *1963*, No. 020071.
(45) Fresno, F.; Tudela, D.; Coronado, J. M.; Fernández-García, M.; Hungría, A. B.; Soria, J. Influence of Sn^{4+} on the structural and electronic properties of $Ti_{1-x}Sn_xO_2$nanoparticles used as photocatalysts. *Phys. Chem. Chem. Phys.* **2006**, *8*, 2421−2430.
(46) Chua, C. S.; Tan, O. K.; Tse, M. S.; Ding, X. Photocatalytic activity of tin-doped TiO_2 film deposited via aerosol assisted chemical vapor deposition. *Thin Solid Films* **2013**, *544*, 571−575.
(47) Arunachalam, A.; Dhanapandian, S.; Manoharan, C. Effect of Sn doping on the structural, optical and electrical properties of TiO_2 films prepared by spray pyrolysis. *J. Mater. Sci.: Mater. Electron.* **2016**, *27*, 659−676.
(48) Chandra, M. R.; Siva Prasada Reddy, P.; Rao, T. S.; Pammi, S. V. N.; Siva Kumar, K.; Vijay Babu, K.; Kiran Kumar, C.; Hemalatha, K. P. J. Enhanced visible-light photocatalysis and gas sensor properties of polythiophene supported tin doped titanium nanocomposite. *J. Phys. Chem. Solids* **2017**, *105*, 99−105.
(49) Liu, J.; Luo, J.; Yang, W.; Wang, Y.; Zhu, L.; Xu, Y.; Tang, Y.; Hu, Y.; Wang, C.; Chen, Y.; Shi, W. Synthesis of Single-Crystalline Anatase TiO_2 Nanorods With High-Performance Dye-Sensitized Solar Cells. *J. Mater. Sci. Technol.* **2015**, *31*, 106−109.
(50) Niu, B.; Wang, X.; Wu, K.; He, X.; Zhang, R. Mesoporous Titanium Dioxide: Synthesis and Applications in Photocatalysis, Energy and Biology. *Materials* **2018**, *11*, 1910.
(51) Khan, S. A.; Ali, S.; Sohail, M.; Morsy, M. A.; Yamani, Z. H. Fabrication of TiO_2/Ag/Ag_2O Nanoparticles to Enhance the Photocatalytic Activity of Degussa P25 Titania. *Aust. J. Chem.* **2016**, *69*, 41−46.
(52) Singaravelan, R.; Bangaru Sudarsan Alwar, S. Electrochemical synthesis, characterisation and phytogenic properties of silver nanoparticles. *Appl. Nanosci.* **2015**, *5*, 983−991.
(53) Liu, Z.; Sun, D. D.; Guo, P.; Leckie, J. O. An Efficient Bicomponent TiO_2/SnO_2 Nanofiber Photocatalyst Fabricated by Electrospinning with a Side-by-Side Dual Spinneret Method. *Nano Lett.* **2007**, *7*, 1081−1085.

https://dx.doi.org/10.1021/acsomega.9b03876
ACS Omega 2020, 5, 6405−6413

(54) Sohail, M.; Sharif, M.; Khan, S. A.; Sher, M.; Jagadeesh, R. V. Method for the synthesis of nanoparticles of heterometallic nanocomposite materials. US Patent App. 15/724,445: 2019.

https://dx.doi.org/10.1021/acsomega.9b03876
ACS Omega 2020, 5, 6405−6413

A Novel Tin-Doped Titanium Oxide Nanocomposite for Efficient Photo-anodic Water Splitting

Manzar Sohail[a*], Nadeem Baig[b], Muhammad Sher[c], Rabia Jamil[a], Muhammad Altaf[e], Sultan Akhtar[d], Muhammad Sharif[b*]

[a]Department of Chemistry, School of Natural Sciences, National University of Sciences and Technology, Islamabad 44000, Pakistan.

[b]Chemistry Department, King Fahd University of Petroleum and Minerals, Dhahran 31261, Saudi Arabia.

[c]Department of Chemistry, Allama Iqbal Open University, Islamabad, Pakistan.

[d]Electron Microscopy Unit, Institute for Research and Medical Consultations, Imam Abdulrahman Bin Faisal University, Dammam 31441, Saudi Arabia.

[e]Department of Chemistry, Government College University, Lahore, Pakistan.

.

*Corresponding author:

Manzar Sohail

Department of Chemistry, School of Natural Sciences, National University of Science and Technology, Islamabad 44000, Pakistan E.mail: Manzar.sohail@sns.nust.edu.pk; Tel. +92-51-9058-5596

Supplementary Information

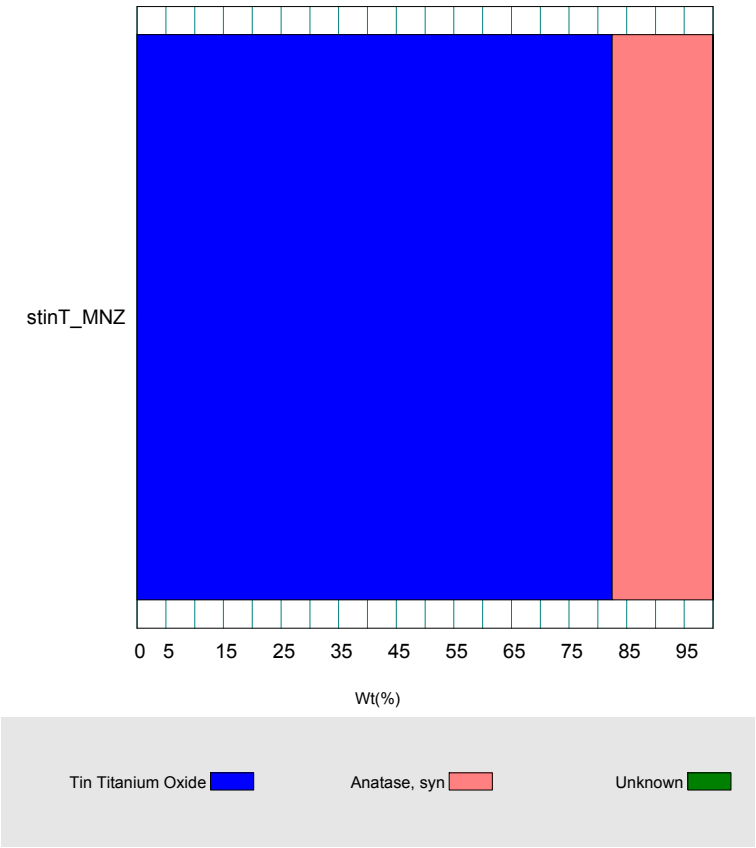

Figure S1. Relative intensity ratio (RIR) analysis from pXRD, of the $Sn_{0.39}Ti_{0.61}O_2.TiO_2$ nanocomposite (Tin Titanium Oxide 82.5 %, TiO_2 (Anatase 17.5 %).

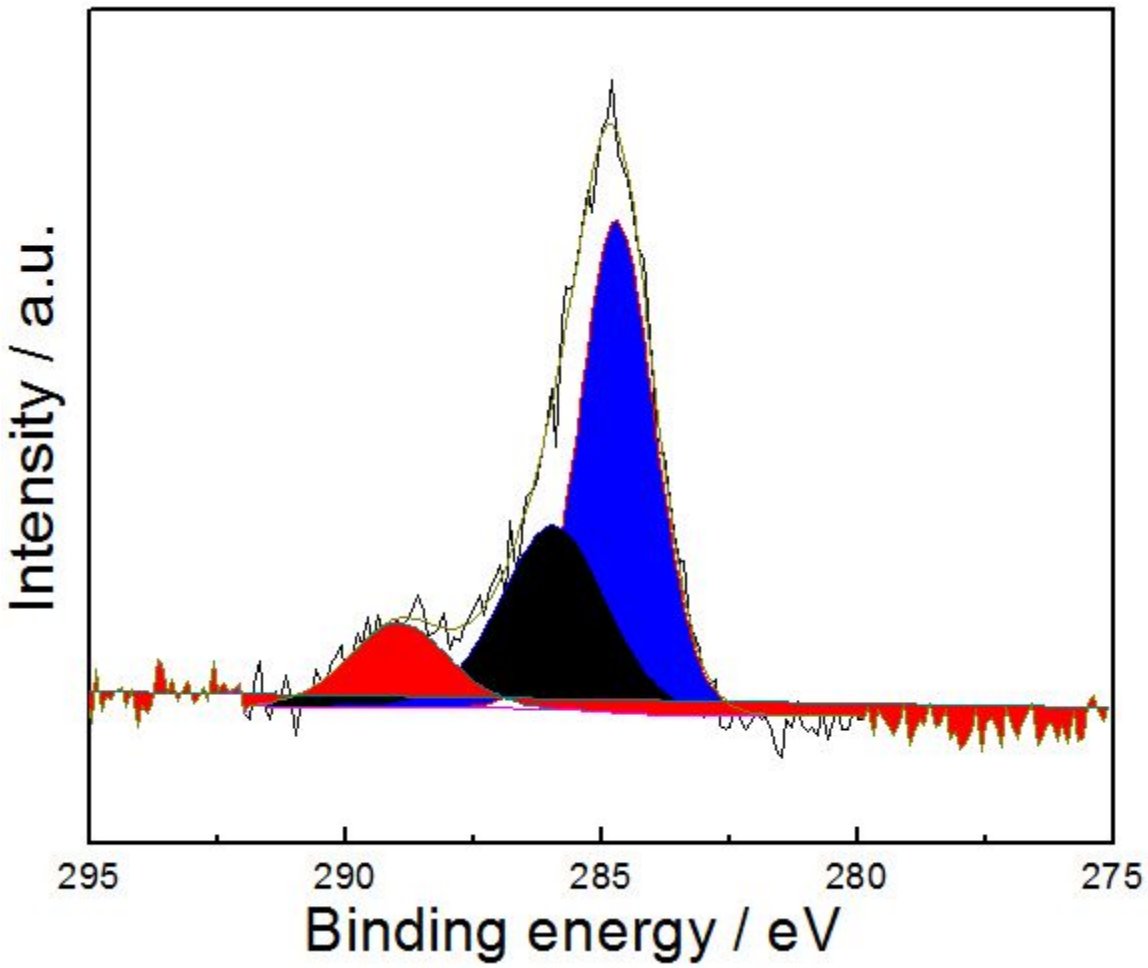

Figure S2. C1s high resolution XPS spectrum

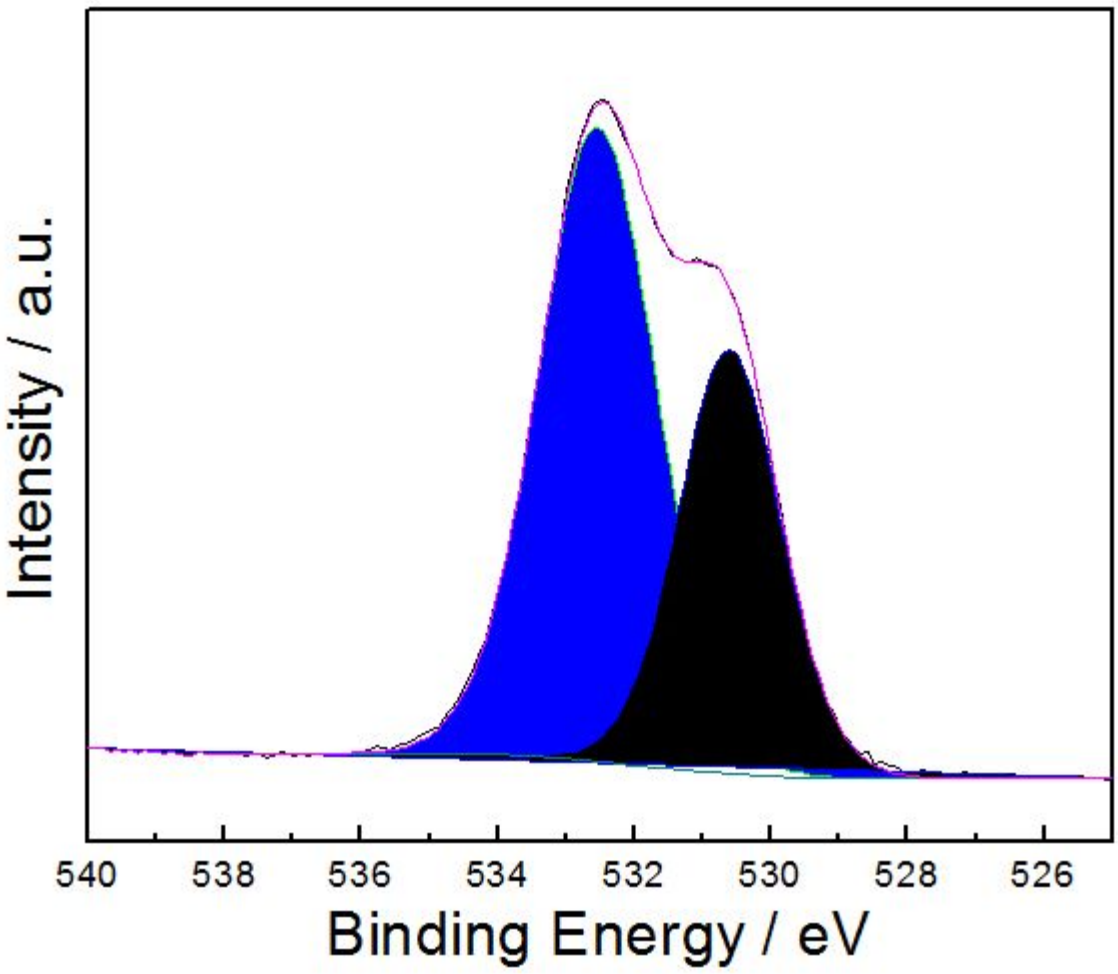

Figure S3. O1s high resolution XPS spectrum

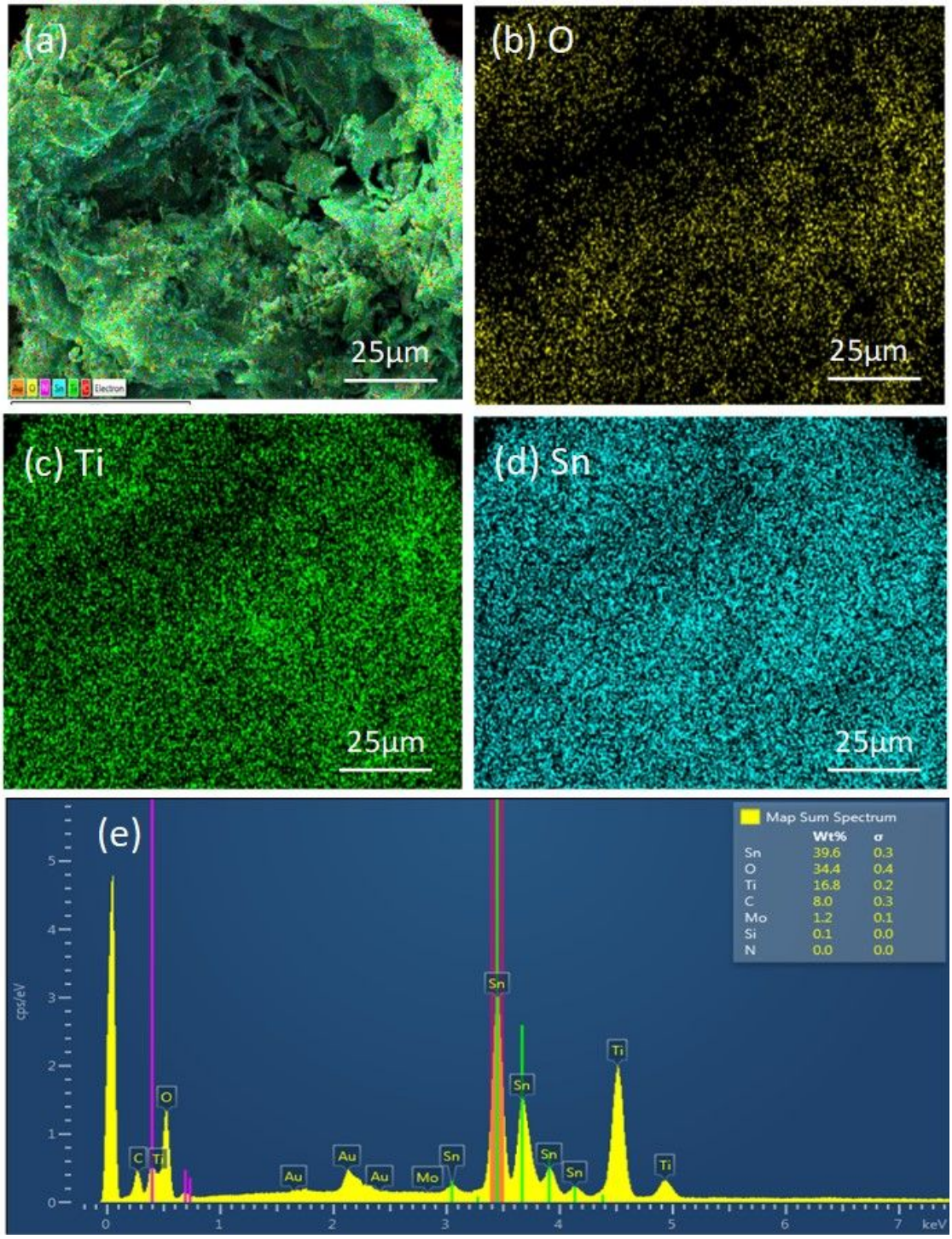

Figure S4. EDX mapping images and EDS spectrum of the $Sn_{0.39}Ti_{0.61}O_2.TiO_2$ composite. EDX mapping of the $SnTiO_2$ photocatalyst demonstrates the uniform distribution of its elements. EDX mapping analysis of (b) Oxygen, (c) Titanium and (d) Tin. EDX spectrum of the synthesized $Sn_{0.39}Ti_{0.61}O_2.TiO_2$ photocatalyst showing the existence of different components, Ti, Sn, and O. The Au peak is appeared due to the gold coating of the specimen.

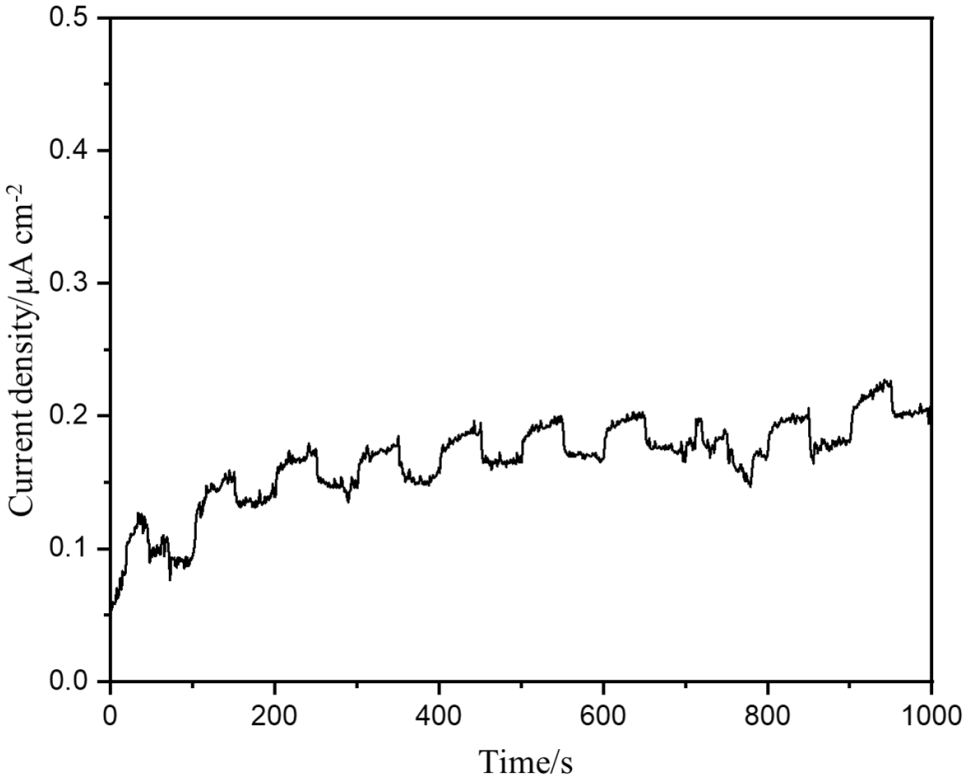

Figure S5 Chronoamperometery in light chopping mode of TiO_2 anatase/ FTO response for OER reaction under dark and light.

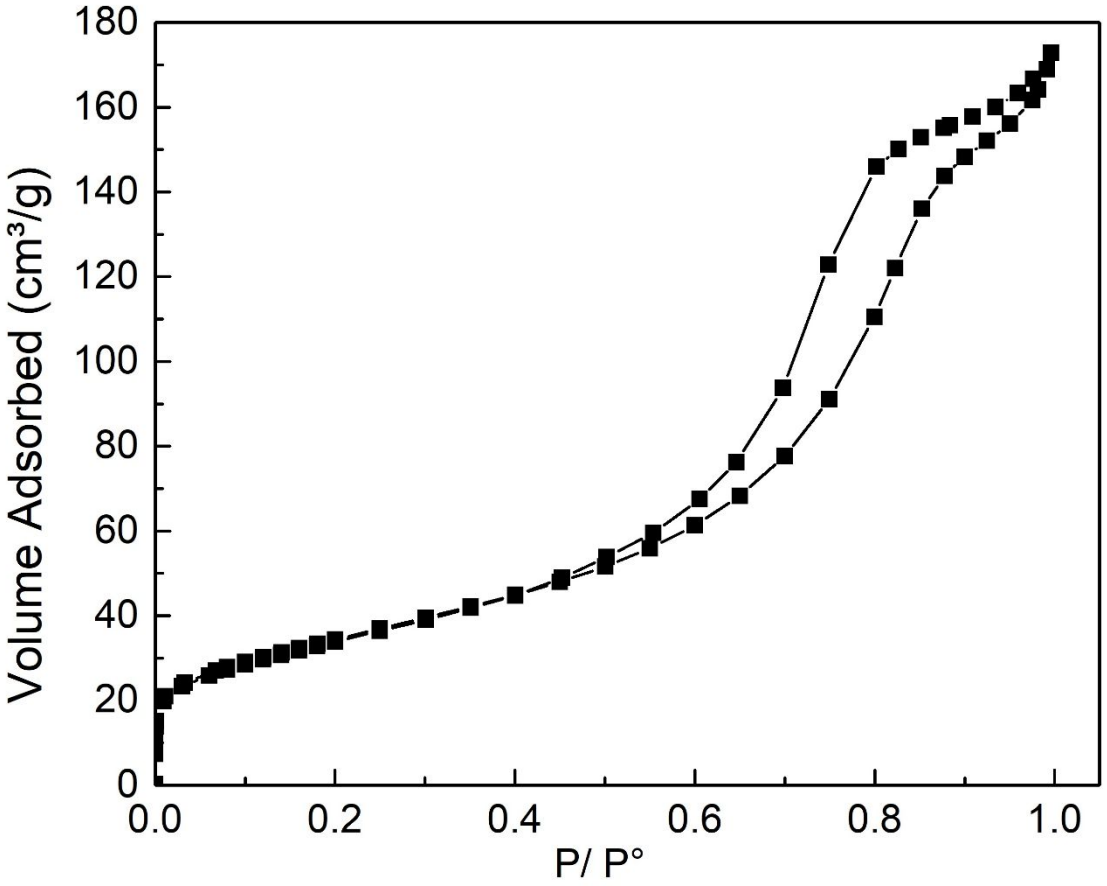

Figure S6. BET adsorption-desorption isotherm graph for $Sn_{0.39}Ti_{0.61}O_2.TiO_2$